Title

Evaluation of Spatial Attentive Deep Learning for Automatic Placental Segmentation on Longitudinal MRI

Journal

Journal of Magnetic Resonance Imaging, 57(5)

ISSN

1053-1807

Authors

Liu, Yongkai
Zabihollahy, Fatemeh
Yan, Ran
et al.

Publication Date

2023-05-01

DOI

10.1002/jmri.28403

Peer reviewed

Evaluation of Spatial Attentive Deep Learning for Automatic Placental Segmentation on Longitudinal MRI

Yongkai Liu, Ph.D.[1,2*], Fatemeh Zabihollahy, Ph.D.[1], Ran Yan, M.S.[1,3], Brian Lee, M.D.[4], Carla Janzen, M.D., Ph.D.[5], Sherin U. Devaskar, M.D.[4], Kyunghyun Sung, Ph.D.[1,2,3]

[1] Department of Radiological Sciences, David Geffen School of Medicine, University of California, Los Angeles, CA, USA
[2] Physics and Biology in Medicine IDP, David Geffen School of Medicine, University of California, Los Angeles, CA, USA
[3] Department of Bioengineering, Henry Samueli School of Engineering, University of California, Los Angeles, CA, USA
[4] Department of Pediatrics, David Geffen School of Medicine, University of California, Los Angeles, CA, USA
[5] Department of Obstetrics and Gynecology, David Geffen School of Medicine, University of California, Los Angeles, CA, USA

Journal: Journal of Magnetic Resonance Imaging
Paper Type: Original Article
Running Head: Automated placenta segmentation with longitudinal MRI

***Correspondence to:**
Yongkai Liu, Ph.D.
Department of Radiological Sciences
300 UCLA Medical Plaza, Suite B114
Los Angeles, CA 90095
Phone: (310) 694-4715
liuyongkai1009@g.ucla.edu

The authors disclose no potential conflicts of interest.

Grant Sponsors: NIH U01-HD087221

ABSTRACT

Background: Automated segmentation of the placenta by MRI in early pregnancy may help predict normal and aberrant placenta function, which could improve the efficiency of placental assessment and the prediction of pregnancy outcomes. An automated segmentation method that works at one gestational age may not transfer effectively to other gestational ages.

Purpose: To evaluate a spatial attentive deep learning method (SADL) for automated placental segmentation on longitudinal placental MRI scans.

Study type: Prospective, single-center.

Subjects: 154 pregnant women who underwent MRI scans at both 14-18 weeks of gestation and at 19-24 weeks of gestation, divided into training (N=108), validation (N=15) and independent testing datasets (N=31).

Field Strength/Sequence: 3T, T2-weighted Half Fourier Single-shot Turbo spin-echo (T2-HASTE) sequence.

Assessment: The reference standard of placental segmentation was manual delineation on T2-HASTE by a 3rd-year neonatology clinical fellow (B.L.) under the supervision of an experienced maternal-fetal medicine specialist (C.J. with 20 years of experience) and an MRI scientist (K.S. with 19 years of experience).

Statistical Tests: The 3D Dice Similarity Coefficient (DSC) was used to measure the automated segmentation performance compared to the manual placental segmentation. A paired t-test was used to compare the DSCs between SADL and U-Net methods. A Bland–

Altman plot was used to analyze the agreement between manual and automated placental volume measurements. A p value < 0.05 was considered statistically significant.

Results: In the testing dataset, SADL achieved average DSCs of 0.83 ± 0.06 and 0.84 ± 0.05 in the first and second MRI, which were significantly higher than those achieved by U-Net (0.77 ± 0.08 and 0.76 ± 0.10, respectively). A total of 6 out of 62 MRI scans (9.6%) had volume measurement differences between the SADL-based automated and manual volume measurements that were out of 95% limits of agreement.

Data Conclusions: SADL can automatically detect and segment the placenta with high performance in MRI at two different gestational ages.

Level of Evidence:

4

Technical Efficacy Stage:

2

Keywords: Automated placental segmentation, spatial attentive deep learning, convolutional neural network.

INTRODUCTION

The placenta is an intrauterine organ necessary for the maintenance of pregnancy [1]. Abnormal placental development can adversely affect maternal health and interfere with nutrient and oxygen transport to the developing fetus. Collectively, aberrant placental development contributes toward perinatal morbidity and mortality through the development of pre-eclampsia (PE) in the mother with or without fetal growth restriction [1, 2]. MRI has been used to detect placental volume and perfusion dysfunction [2, 3].

Segmentation of the placenta by MRI is the first step required for the accurate detection of volumetric abnormalities that can affect maternal and fetal health [4] [5]. Manual segmentation of the placenta involves delineation of multiple 2D MRI placental slices that contribute toward the placenta volume. This process is time-consuming and may result in large inter-and intra-individual reader variability [6]. Automated segmentation would enable rapid tissue segmentation and overcome the subjectivity associated with manual segmentation.

In recent years, machine learning and deep learning (DL) have demonstrated superior capabilities in medical image segmentation [1, 7–17]. For placental segmentation in MRI, Wang et al. [18] have developed an online learning-based method [19]. In addition, Alansary et al. [16] have implemented a 3D multi-scale convolutional neural network (CNN) with 3D dense conditional random fields. Wang et al. [8, 17] have also developed a DL-based interactive framework that integrated user interaction with CNN, while Han et al. [9] and Shahedi et.al [1] have evaluated U-Net variants.

These studies were either evaluated in scans at a single and late gestational age (GA) or were not fully automated workflows. The placenta is constantly evolving and growing throughout pregnancy. Consequently, an automated segmentation model working in late gestation pregnancy MRI may not transfer effectively for use during early pregnancy MRI. In addition, a single placental MRI scan could comprise multiple image slices that could contain or not contain the placenta. Manual operations and interactions such as selecting image slices containing the placenta could contribute toward significant subjectivity and increase the cognitive workload on experts. Thus, the aim of this study was to evaluate an end-to-end, fully automated segmentation workflow, spatial attention deep learning method (SADL), for placental segmentation using MRIs obtained at two time-points during early pregnancy and to (1) compare the segmentation performance with the state-of-the-art DL-based method, U-Net; and (2) compare placenta volume measurements obtained by manual and automated SADL methods.

MATERIALS AND METHODS

Subject Population and MRI Dataset

This study was carried out according to the United States Health Insurance Portability and Accountability Act (HIPAA) of 1996 with approval from the institutional review board (IRB), and all subjects provided written informed consent. We approached all eligible pregnant women entering prenatal care in the first trimester of pregnancy at the local antenatal clinic without pre-selection. Inclusion criteria were a gestational age of less than 14 weeks, age more than 18 years old, pregnancy with a single fetus, the absence of fetal

chromosomal or structural abnormalities, no treatment with aspirin, heparin, or antihypertensive drugs before enrollment, the ability to provide consent, a non-smoker, and planning to deliver at the same local institution. Exclusion criteria included abortion (spontaneous or planned termination), loss of follow-up, withdrawal from the study, and a history of diabetes mellitus. Gestational age was confirmed by a dating ultrasound scan in the first trimester of pregnancy.

The longitudinal MRI scans were acquired at 14-18 weeks (first MRI) and 19 to 24 weeks (second MRI) gestational age. A T2-weighted Half-Fourier Single Shot Turbo Spin Echo (T2 HASTE) [20] sequence was used to acquire placental MRI on one of two 3.0 T MRI scanners (Prisma and Skyra; Siemens Healthcare, Erlangen, Germany). Detailed sequence parameters for T2-HASTE are described in Table 1. The T2 HASTE MR images were acquired in three orthogonal imaging planes (axial, sagittal, and coronal). Image analysis was performed using the open-source image analysis OsiriX MD software package (version 11.0.3, Pixmeo SARL, Geneva, Switzerland). Regions of interest (ROIs) were manually drawn around the placenta in each imaging plane as ground truth. A 3rd-year neonatology fellow (B.L.) supervised by an MRI scientist (K.S. with 19 years of experience) manually defined the ROIs on each of the T2-HASTE MRI slices that included placenta. The clinical fellow was also supervised by an obstetrician-gynecologist (C.J. with 20 years of experience) who is a specialist in maternal and fetal medicine whenever the placental anatomy was considered challenging to segment. Figure 1 shows a representative example of manual placental segmentation in the three orthogonal planes. The placenta volumes

measured in the three orthogonal imaging planes were averaged to minimize potential error due to low through-plane resolution on T2 HASTE MRI images.

Proposed Spatial Attentive Deep Learning

The structure of the proposed SADL is shown in Figure 2. The whole network is comprised of a spatial attentive deep residual network (based on the ResNet50) [21] as the encoder, a feature pyramid attention (FPA) module [22] to enhance capturing multi-scaled information, and a naïve decoder network to recover spatial resolution. Inside the encoder, the modifications were twofold: 1) A criss-cross (CC) spatial attention module [23] was added at the beginning of the ResNet50, which helped the network emphasize areas with more semantic features of the placenta by modeling spatial dependent information via the global features. Specifically, each pixel's response was obtained by considering all the pixels so that more importance was adaptively given to pixels with more semantic information; and 2) MaxPool was removed from the original ResNet50. Several studies [12, 24] have shown that the inclusion of MaxPool compromises image segmentation performance. Next, an FPA network was added after the encoder, thereby furthering the enhancement of multi-scaled feature extraction. Finally, a naïve decoder was connected to the FPA to recover the spatial resolution.

Baseline method - U-Net

U-Net is a fully convolutional neural network, which was proposed by Ronneberger and Olaf et al and popularized for biomedical image segmentation. U-Net includes an encoder to extract high-level features and a decoder to recover the spatial resolution compromised in

the encoder. The classic U-Net framework, which can be seen in Figure 3, served as the baseline to compare with the proposed method.

Experimental Setups – Training and Testing

All deep learning models were implemented using Pytorch, and the placental volume was calculated using Pyradiomics [25]. We divided the study cohort into training (n=108; 70%), validation (n=15; 10%), and testing (n=31; 20%) sets. We used stochastic gradient descent (SGD) as an optimizer and a binary cross-entropy as the loss function for the deep learning model training. The network was trained for 200 epochs and the model with the lowest validation loss was selected as the optimal model for placenta segmentation. Finally, the optimal model was evaluated using the testing set of MRIs. The image slices in the three views were cropped to a matrix size of 256 × 256 in the central region. The bounding box contained all placental structures in the images obtained from each view. In-fly data augmentation techniques included random rotations between [−5°, 5°], elastic transformations, random contrast adjustment, and random horizontal flip. We also performed image normalization to reduce skewing. Each placental MRI scan contained three imaging planes (axial, coronal, and sagittal). To make the model capable of segmenting placental MRI images in different imaging planes (axial, coronal, and sagittal), we included the images from all three views to train the model. All slices, including those with and without the placenta, were fed into the models to help the network learn the placenta span. The segmentation performance of the SADL model was compared with that of the U-Net model in the testing data set. Segmentation performance was assessed for first and second MRI scans separately and in combination. Segmentation performance was also assessed for

each image orientation separately and in combination. In addition, volumes from automated SADL segmentations were compared to those from manual segmentations.

Statistical Analysis

The 3D Dice Similarity Coefficient (DSC) [26] was used to measure the segmentation performance in the testing set, formulated as:

$$DSC = \frac{2|A \cap B|}{|A \cup B|} \quad (1)$$

where A and B are automated and manual 3D segmentations of the placenta, respectively. DSC of each MRI scan was calculated by averaging the DSCs from the three orthogonal imaging planes (axial, sagittal, and coronal). The significance of differences in DSC obtained using SADL and the baseline U-Net method was investigated using a paired sample t-test at the 95% level of confidence. A Bland–Altman plot [27] was used to analyze the agreement between manual and automatic placental volume measurements. Linear regression models [28] were used to model the relationships between the volume size and age under manual and automated placental volume measurements.

RESULTS

A total of 154 pregnant women who completed two MRI scans during the second trimester were recruited between 2016 and 2019. The summary of the study subjects' characteristics is shown in Table 2. Figure 4 shows a representative example of automated placenta segmentation by SADL and U-Net. Table 3 shows the DSC comparison between SADL and U-Net in the testing dataset. In the first and second MRI scans, SADL achieved average

DSCs of 0.83 ± 0.06 and 0.84 ± 0.05 respectively. These were significantly higher than those achieved by U-Net (0.77 +/- 0.08 and 0.76 +/- 0.10, respectively). SADL performed similarly between the first and second MRI (0.83 ± 0.06 vs. 0.84 ± 0.05; p=0.47). Representative examples of excellent and poor placental segmentation of MRI images using SADL and U-Net are shown in Figure 5.

Table 4 shows the DSC by SADL and U-Net across the three different orthogonal planes. At the first MRI, SADL achieved similar DSCs across the three orthogonal imaging planes (0.83, 0.83, and 0.82 for axial, coronal, and sagittal planes). However, at the second MRI, the SADL achieved a DSC of 0.87 ± 0.03 at the axial plane, which was significantly higher than those of other imaging planes (0.82 ± 0.10 and 0.83 ± 0.07 for coronal and sagittal planes; both p values are 0.01). In addition, we found SADL significantly outperformed U-Net across each imaging plane at both first and second MRIs.

Figure 6 shows the agreement between manual and SADL-based automated volume measurements in a Bland–Altman plot. The mean difference (bias) was 1.04 ml and the 95% limits of agreement (average difference ± 1.96 SD) were -52.45 ml to 55.14 ml. It turned out that 6 out of 62 MRI scans (9.6%) had the volume measurement differences that were beyond the 95% limits of agreement.

Figure 7 shows the similar linear regression models between the placental volume size and the gestational ages for SADL-based automated (Figure 6 (A)) and manual (Figure 6 (B)) volume calculations.

Table 6 shows the placental segmentation performance of SADL at different positions such as anterior and posterior. Based on the table, posterior placentas exhibited a

slightly higher DSC than anterior ones at the first and second MRI. However, there was no significant difference between the anterior and posterior placenta's segmentation performance at both MRIs.

DISCUSSION

We developed a novel method, SADL, for automated segmentation of the placenta from two longitudinal MRI scans, taken at 14-18 and at 19-24 weeks of gestation. Our results demonstrated that accurate contouring of the placenta on both MRIs is feasible. The proposed method is fully automated; thus, the results are reproducible. Our suggested methodology outperformed a U-Net based model which is currently state-of-the-art for placenta delineation from MRI [1, 9].

Our model is equipped with a CC spatial attentive module [23] that requires less GPU memory than the regular spatial attentive module [23]. In the CC spatial attentive module, the response of each pixel only considers the pixels on its criss-cross path rather than all the pixels in the image, which reduces the amount of GPU memory required. A CC spatial attentive module could provide an alternative to the regular spatial attention module when the GPU memory available is limited.

Compared with Han et al.'s deep learning-based method [9] for placenta MRI segmentation, our work differs in the following aspects: 1) We had a larger data set containing MRI of 154 subjects, from which 31 images were used as an independent test set; 2) Our model is fully automated where the whole images are fed to the network for placental segmentation while in the method proposed by Han et al., the user first needs to determine

the extent of the placenta on MRI; 3) Our study conducted a patient-wise segmentation evaluation compared to the image-wise segmentation evaluation in their study; and 4) Dataset used in our study included MRI scans obtained at two gestational ages, which we used to explore the performance of the segmentation model across multiple gestational ages;

We found that the model trained using both MRIs (first and second) achieved better segmentation performance than the one trained only using the first or the second MRIs. Since the placenta is a temporary human organ that varies substantially during early gestation, using the first and second MRI together during the training increased the amount and type of training samples of placental MRI, which could have improved the model's ability to recognize different-sized placental regions. The consistent segmentation performance in the MRI at two different early GAs also suggests that the model potentially provides robust segmentation across differing longitudinal MRI scans during early gestation.

Our findings indicated that the relationship between volume and gestational age was maintained between manual and automated volume calculations. This could benefit future studies that require such relationships for the detection of placental volume-related disease models. Examples of such diseases include gestational diabetes mellitus or ischemic placental disease [29, 30].

To investigate SADL's generalizability to other organs, we also trained and tested a SADL model for prostate whole gland segmentation. SADL achieved an average DSC of 0.92 ± 0.03 in a testing dataset including 31 prostate MRI scans.

Limitations

Our study still has a few limitations. First, ground truth of manual segmentations was performed by a single observer. In the future, we will recruit more observers to annotate the placenta and analyze the interobserver variability between among them. Second, the SADL model is a 2D-based deep learning model, which does not retain the inter-slice correlation information as in 3D placental images. We will explore ways to develop a 3D-based model to better capture the inter-slice correlation information in the future. Third, all images were obtained from a single medical center, which may introduce population bias. Fourth, the same placental MRI protocol with a single vendor was used for acquiring placental MRI images for all scans. In the future, datasets from multiple institutions and vendors will be integrated to test the generalizability of our developed automated placenta segmentation method.

Conclusions

In conclusion, we proposed a spatial attentive deep learning network, SADL, for automated segmentation of the placenta during the second trimester. SADL can automatically segment the placenta in placenta MRI at different gestational ages during the second trimester. In addition, the difference between automated placental volume measurement with the SADL-based segmentation and manual volume measurement was small.

REFERENCES

1. Shahedi M, Dormer JD, Tensingh Rajan Thanga Kani AD, Do QN, Xi Y, Lewis MA, Madhuranthakam AJ, Twickler DM, Fei B (2020) Segmentation of uterus and placenta in MR images using a fully convolutional neural network. Event SPIE Med. Imaging. p 59
2. Liu D, Shao X, Danyalov A, Chanlaw T, Masamed R, Wang DJJ, Janzen C, Devaskar SU, Sung K (2020) Human placenta blood flow during early gestation with pseudocontinuous arterial spin labeling MRI. J Magn Reson Imaging 51:1247–1257.
3. Sorensen AV, Hutter JM, Grant EP, Seed M, Gowland P (2019) T2* weighted placental MRI: basic research tool or an emerging clinical test of placental dysfunction? Ultrasound Obstet. Gynecol.
4. Wenger E, Mårtensson J, Noack H, Bodammer NC, Kühn S, Schaefer S, Heinze H-J, Düzel E, Bäckman L, Lindenberger U, others (2014) Comparing manual and automatic segmentation of hippocampal volumes: reliability and validity issues in younger and older brains. Hum Brain Mapp 35:4236–4248.
5. Maldjian C, Adam R, Pelosi M, Pelosi III M, Rudelli RD, Maldjian J (1999) MRI appearance of placenta percreta and placenta accreta. Magn Reson Imaging 17:965–971.
6. Dahdouh S, Andescavage N, Yewale S, Yarish A, Lanham D, Bulas D, du Plessis AJ, Limperopoulos C (2018) In vivo placental MRI shape and textural features predict fetal growth restriction and postnatal outcome. J Magn Reson Imaging 47:449–458.
7. Ronneberger O, Fischer P, Brox T (2015) U-net: Convolutional networks for biomedical image segmentation. Int. Conf. Med. image Comput. Comput. Interv. pp 234–241
8. Wang G, Li W, Zuluaga MA, Pratt R, Patel PA, Aertsen M, Doel T, David AL, Deprest J, Ourselin S, Vercauteren T (2018) Interactive Medical Image Segmentation Using Deep Learning with Image-Specific Fine Tuning. IEEE Trans Med Imaging 37:1562–1573.
9. Han M, Bao Y, Sun Z, Wen S, Xia L, Zhao J, Du J, Yan Z (2019) Automatic Segmentation of Human Placenta Images with U-Net. IEEE Access 7:180083–180092.
10. Milletari F, Navab N, Ahmadi SA (2016) V-Net: Fully convolutional neural networks for volumetric medical image segmentation. Proc. - 2016 4th Int. Conf. 3D Vision, 3DV 2016. Institute of Electrical and Electronics Engineers Inc., pp 565–571
11. Havaei M, Davy A, Warde-Farley D, Biard A, Courville A, Bengio Y, Pal C, Jodoin PM, Larochelle H (2017) Brain tumor segmentation with Deep Neural Networks. Med Image Anal 35:18–31.
12. Liu Y, Yang G, Mirak SA, Hosseiny M, Azadikhah A, Zhong X, Reiter RE, Lee Y, Raman SS, Sung K (2019) Automatic Prostate Zonal Segmentation Using Fully Convolutional Network With Feature Pyramid Attention. IEEE Access 7:163626–163632.
13. Liu Y, Yang G, Hosseiny M, Azadikhah A, Mirak SA, Miao Q, Raman SS, Sung K (2020) Exploring Uncertainty Measures in Bayesian Deep Attentive Neural Networks for Prostate Zonal Segmentation. IEEE Access 8:151817–151828.
14. Looney P, Stevenson GN, Nicolaides KH, Plasencia W, Molloholli M, Natsis S, Collins SL (2018) Fully automated, real-time 3D ultrasound segmentation to estimate first trimester placental volume using deep learning. JCI insight. doi: 10.1172/jci.insight.120178

15. Hu R, Singla R, Yan R, Mayer C, Rohling RN (2019) Automated Placenta Segmentation with a Convolutional Neural Network Weighted by Acoustic Shadow Detection. Proc. Annu. Int. Conf. IEEE Eng. Med. Biol. Soc. EMBS. Institute of Electrical and Electronics Engineers Inc., pp 6718–6723

16. Alansary A, Kamnitsas K, Davidson A, Khlebnikov R, Rajchl M, Malamateniou C, Rutherford M, Hajnal J V., Glocker B, Rueckert D, Kainz B (2016) Fast fully automatic segmentation of the human placenta from motion corrupted MRI. Lect. Notes Comput. Sci. (including Subser. Lect. Notes Artif. Intell. Lect. Notes Bioinformatics). Springer Verlag, pp 589–597

17. Wang G, Zuluaga MA, Li W, Pratt R, Patel PA, Aertsen M, Doel T, David AL, Deprest J, Ourselin S, Vercauteren T (2019) DeepIGeoS: A Deep Interactive Geodesic Framework for Medical Image Segmentation. IEEE Trans Pattern Anal Mach Intell 41:1559–1572.

18. Wang G, Zuluaga MA, Pratt R, Aertsen M, David AL, Deprest J, Vercauteren T, Ourselin S (2015) Slic-seg: Slice-by-slice segmentation propagation of the placenta in fetal MRI using one-plane scribbles and online learning. Lect. Notes Comput. Sci. (including Subser. Lect. Notes Artif. Intell. Lect. Notes Bioinformatics). Springer Verlag, pp 29–37

19. Wang G, Zuluaga MA, Pratt R, Aertsen M, Doel T, Klusmann M, David AL, Deprest J, Vercauteren T, Ourselin S (2016) Slic-Seg: A minimally interactive segmentation of the placenta from sparse and motion-corrupted fetal MRI in multiple views. Med Image Anal 34:137–147.

20. Patel MR, Klufas RA, Alberico RA, Edelman RR (1997) Half-fourier acquisition single-shot turbo spin-echo (HASTE) MR: Comparison with fast spin-echo MR in diseases of the brain. Am J Neuroradiol 18:1635–1640.

21. He K, Zhang X, Ren S, Sun J (2016) Deep residual learning for image recognition. Proc. IEEE Conf. Comput. Vis. pattern Recognit. pp 770–778

22. Li H, Xiong P, An J, Wang L (2018) Pyramid Attention Network for Semantic Segmentation.

23. Huang Z, Wang X, Huang L, Huang C, Wei Y, Liu W (2019) Ccnet: Criss-cross attention for semantic segmentation. Proc. IEEE/CVF Int. Conf. Comput. Vis. pp 603–612

24. Ghafoorian M, Karssemeijer N, Heskes T, van Uden IWM, Sanchez CI, Litjens G, de Leeuw F-E, van Ginneken B, Marchiori E, Platel B (2017) Location sensitive deep convolutional neural networks for segmentation of white matter hyperintensities. Sci Rep 7:1–12.

25. Van Griethuysen JJM, Fedorov A, Parmar C, Hosny A, Aucoin N, Narayan V, Beets-Tan RGH, Fillion-Robin J-C, Pieper S, Aerts HJWL (2017) Computational radiomics system to decode the radiographic phenotype. Cancer Res 77:e104--e107.

26. Dice LR (1945) Measures of the Amount of Ecologic Association Between Species. Ecology 26:297–302.

27. Giavarina D (2015) Understanding bland altman analysis. Biochem medica 25:141–151.

28. Leatherbarrow RJ (1990) Using linear and non-linear regression to fit biochemical data. Trends Biochem Sci 15:455–458.

29. Metzenbauer M, Hafner E, Hoefinger D, Schuchter K, Stangl G, Ogris E, Philipp K (2001) Three-dimensional ultrasound measurement of the placental volume in early pregnancy: Method and correlation with biochemical placenta parameters. Placenta 22:602–605.

30. Adams T, Yeh C, Bennett-Kunzier N, Kinzler WL (2014) Long-term maternal morbidity and mortality associated with ischemic placental disease. Semin. Perinatol. pp 146–150

TABLES

Table 1. Detailed T2-HASTE MRI sequence parameters.

Parameter	Value
TE/TR (msec)	92 / 3000
Flip Angle (degree)	150
Bandwidth (Hz/pixel)	390
Resolution ($mm_x \times mm_y$)	0.976 × 0.976
Slice Thickness (mm)	5
Echo Train Length	70
Matrix ($N_x \times N_y$)	272 × 512
Field of View ($mm_x \times mm_y$)	265 × 500

Table 2. Summary of the characteristics of the subjects with pregnancies.

		Total	Training	Validation	Testing
No. of Patients		154	108	15	31
Age, yr. (IQR)		32.9[1] (30-35)[2]	33 (30-35)	33 (30-35)	32 (30-34)
Weight, kg. (IQR)		67.2 (58.5-73.0)	67.1 (58.3-72.7)	67.0 (58.3-72.1)	67.5 (59.1-74.5)
GA[3] at the first MRI, weeks (IQR)		15.7 (15.0-16.3)	15.6 (14.9-16.3)	15.8 (15.3-16.5)	15.8 (15.1-16.0)
GA at the second MRI, weeks (IQR)		20.7 (19.9-21.3)	20.7 (19.9-21.3)	20.6 (19.9-20.8)	20.9 (20.1-21.3)
MRI scans	No. of first MRIs	154	108	15	31
	No. of second MRIs	154	108	15	31
No. of MRI slices		42,553	29,896	4,162	8,495

[1]Mean; [2]Interquartile range; [3]Gestational age

Table 3. DSC comparisons between SADL and U-Net in the testing dataset (N=31).

Methods	DSC	
SADL	0.83 ± 0.06	
	First MRI	Second MRI
	0.83 ± 0.06	0.84 ± 0.05
	p^1=0.47	
U-Net	DSC	
	0.76 ± 0.09 p^2<0.05	
	First MRI	Second MRI
	0.77 ± 0.08 p^2<0.05	0.76 ± 0.10 p^2<0.05

p^1 value is the comparison between the first and second MRI; p^2 values are the comparisons between the SADL and the U-Net.

Table 4. Segmentation Performance of SADL in the three orthogonal views in the testing dataset (N=31).

Methods		Ax	Cor	Sag
SADL	First MRI	0.83 ± 0.06	0.83 ± 0.07	0.82 ± 0.12
	Second MRI	0.87 ± 0.03	0.82 ± 0.10	0.83 ± 0.07
U-Net	First MRI	0.79 ± 0.06 p<0.5	0.78 ± 0.09 p<0.5	0.74± 0.15 p<0.5
	Second MRI	0.84 ± 0.04 p<0.5	0.77 ± 0.10 p<0.5	0.67 ± 0.25 p<0.5

Cor, Sag and Ax are abbreviated for the coronal, sagittal and Axial planes, respectively.
P values are the comparisons between the SADL and the U-Net.

Table 5. Testing of SADL trained with different combinations of MRI

	Model Trained using the first MRI	Model Trained using the second MRI	Model Trained using both MRI
Testing on the first MRI	0.81 ± 0.06	0.77 ± 0.09	0.83 ± 0.06
Testing on the second MRI	0.81 ± 0.06	0.76 ± 0.13	0.84 ± 0.05

Table 6. Placental Segmentation Performance of SADL at Different Positions

	Anterior	Posterior
First MRI	0.82±0.07 (n=19)	0.86±0.02 (n=13)
	p=0.08	
Second MRI	0.82±0.05 (n=18)	0.84±0.04 (n=14)
	p=0.42	

FIGURE CAPTIONS

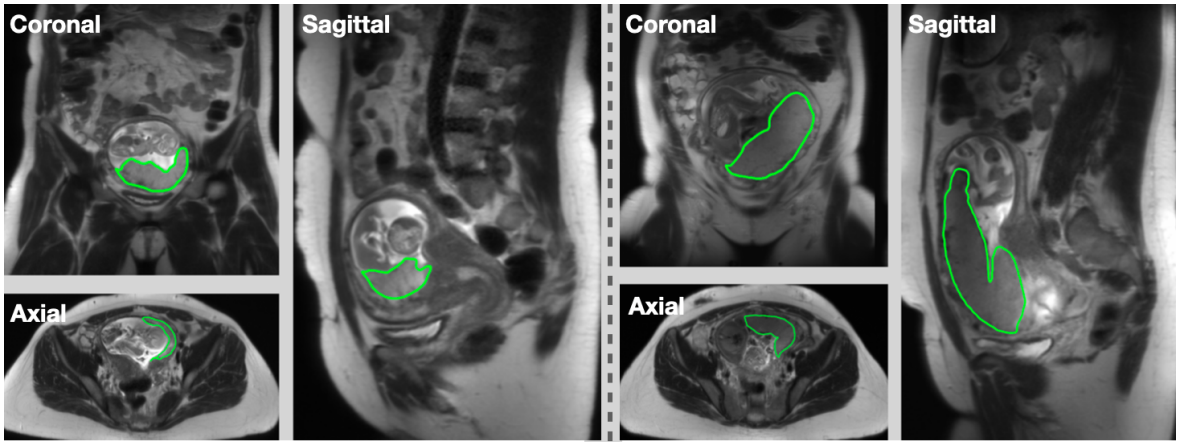

FIGURE 1. Representative placental MRI images in three imaging planes at the first MRI at 15.3 weeks (left; volume = 119cm^3) and second MRI at 21.3 weeks (right; volume = 270cm^3). The placenta was manually contoured and shown as the green line.

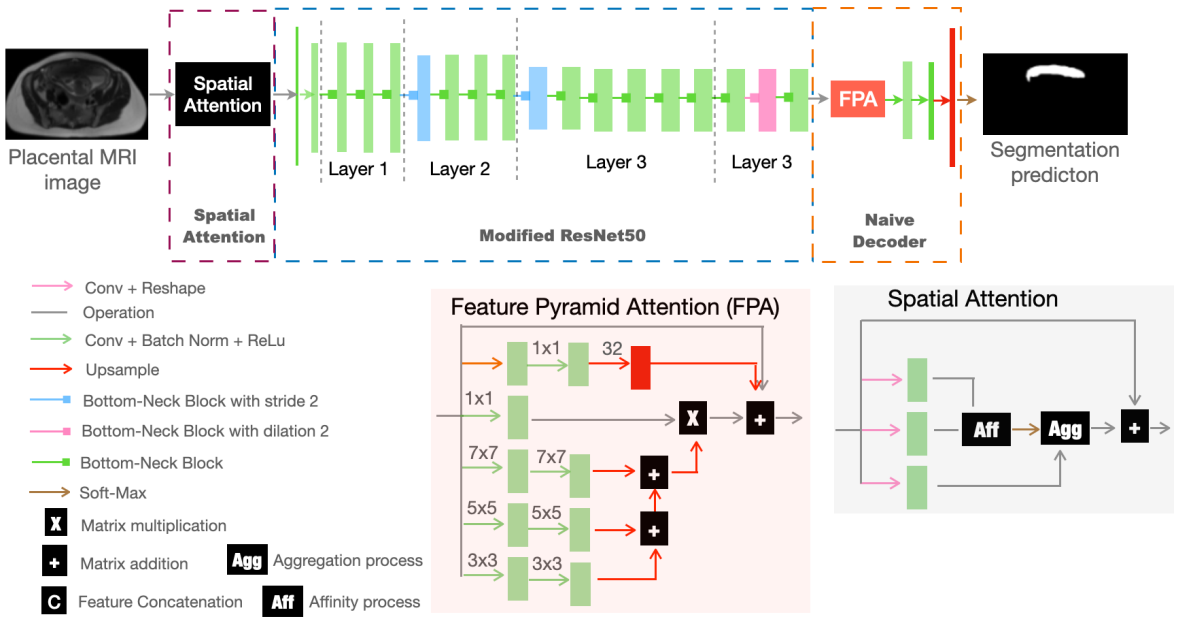

FIGURE 2. An overall structure of the proposed SPDL network. The network consists of 4 sub-networks: a spatial attention module, an improved attentive ResNet50, a feature pyramid attention, and a naïve decoder. The input and output are a 2D placental MRI slice and a placental segmentation prediction. Aggregation and affinity processes were defined in [23].

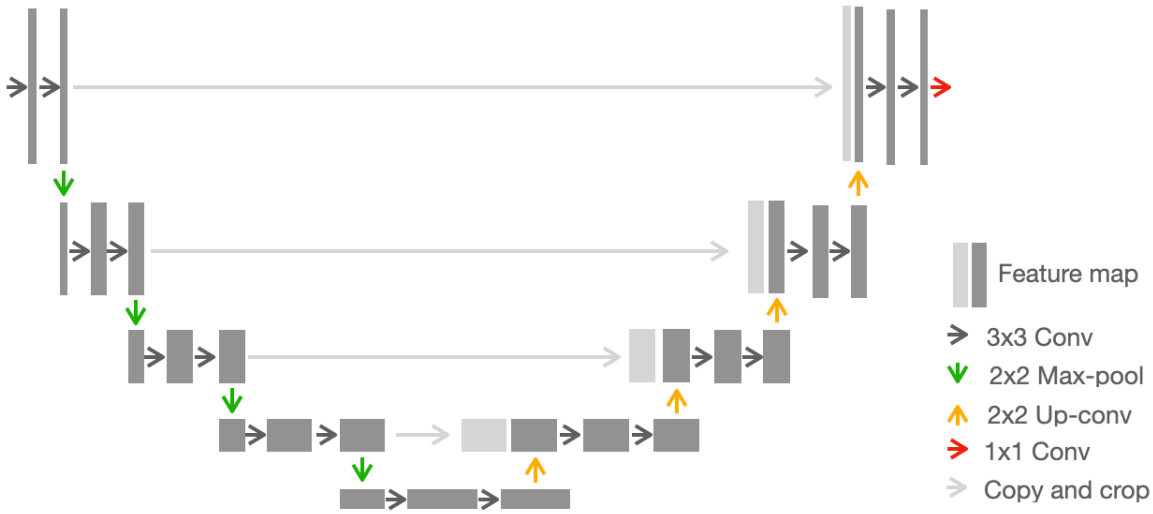

FIGURE 3. Structure of the baseline method – U-Net. Each gray box represents a feature map.

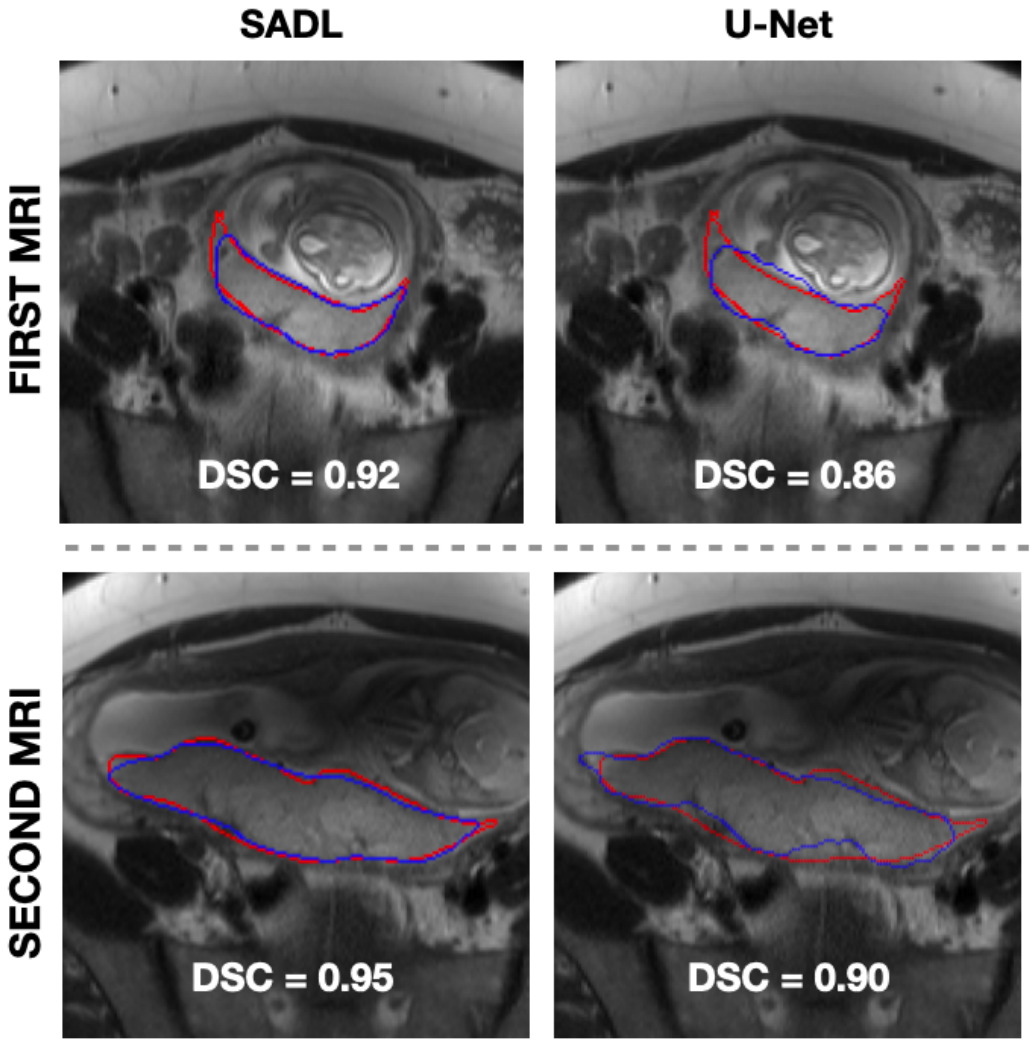

FIGURE 4. Representative example of automated segmentation by SADL and U-Net (blue lines) compared to the manual segmentation (red lines) at the first MRI (*GA = 15 weeks and 1 day*) and the second MRI (*GA = 19 weeks and 4 days*). DSCs are shown below.

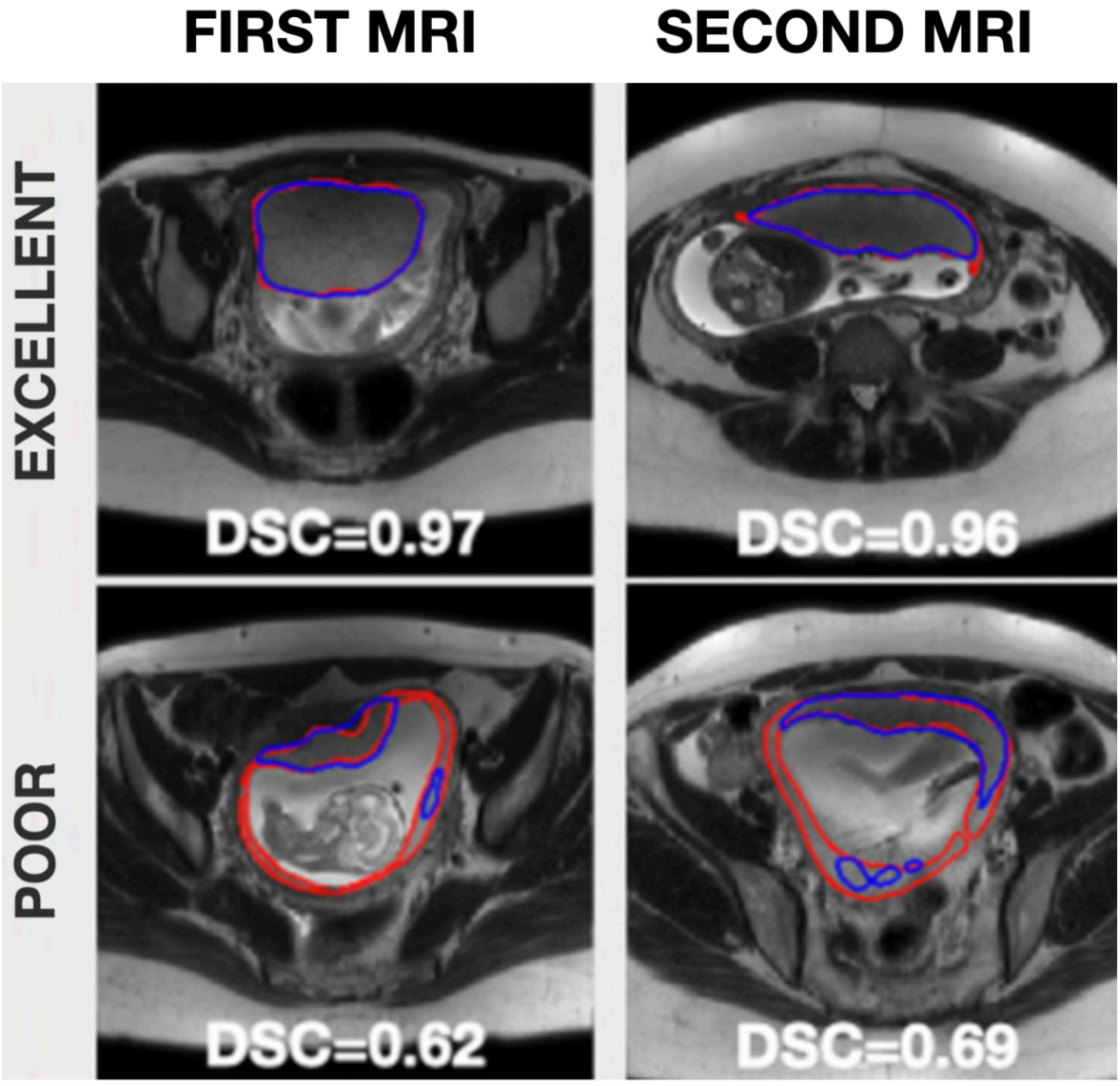

FIGURE 5. Representative examples of excellent and poor automated placental segmentation at the first MRI scan (GA between 14-18 weeks) and the second MRI scan (GA between 14-18 weeks) by the proposed method. Red and blue lines are manual and automated segmentation.

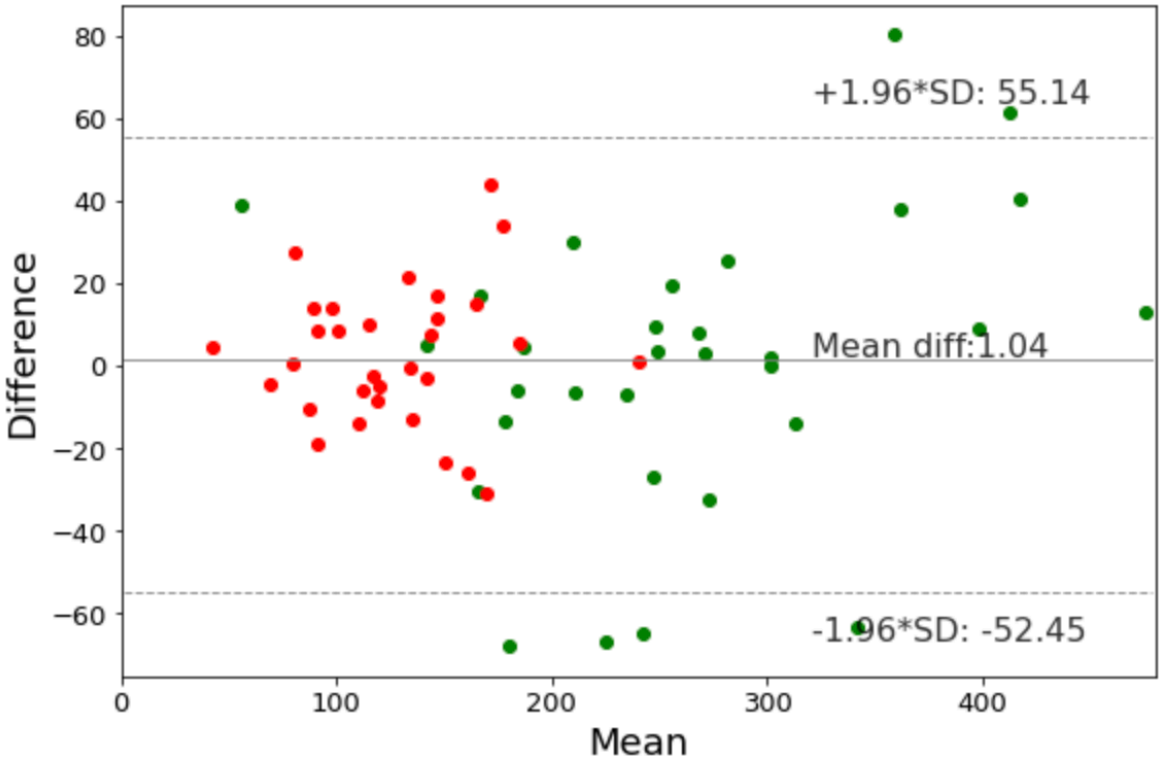

FIGURE 6. A Bland-Altman plot showing the agreement between the automated and manual placental volume measurement. Red and green points represent the first and second MRIs, respectively.

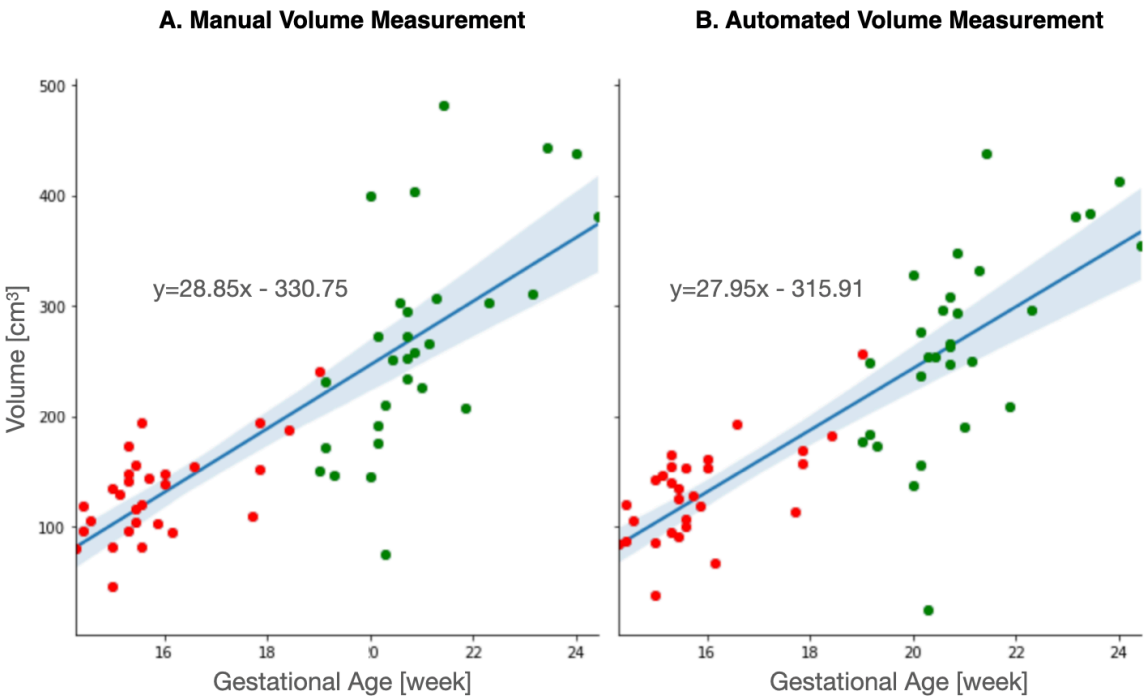

FIGURE 7. Linear regression models between placental volume and gestational age with the manual (A) and automated (B) segmentation. Red and green points are the volume measurements for the first and second MRIs. Blue lines represent the linear regression models between placental volume and gestational age.